

Measurement circuit ansatz: Naimark versus quantum neural-network measurements

Sung Won Yun,¹ Thi Ha Kyaw,² and Joonwoo Bae³

¹Information & Electronics Research Institute, Korea Advanced Institute of Science and Technology (KAIST),
291 Daehak-ro, Yuseong-gu, Daejeon 34141, Republic of Korea

²LG Electronics Toronto AI Lab, Toronto, Ontario M5V 1M3, Canada

³School of Electrical Engineering, Korea Advanced Institute of Science and Technology (KAIST),
291 Daehak-ro, Yuseong-gu, Daejeon 34141, Republic of Korea

In this work, we present constructions of quantum circuits to implement general measurements on quantum hardware. Firstly, we investigate a quantum circuit ansatz by following the Naimark extension with a universal set of gates, such as controlled-NOT and single-qubit gates; we call it a Naimark quantum measurement. We present a circuit ansatz framed by the Naimark extension, leaving single-qubit gates with parameters, and apply a classical optimizer to determine their parameters to approximate a desired quantum measurement. Secondly, we relax the Naimark measurement with quantum neural-network (QNN) circuits, employing parameterized quantum circuits. We present hybrid Naimark-QNN measurements by incorporating QNN circuits into Naimark measurements. Thirdly, we also consider fully QNN measurements with shallow parameterized circuits. Then, we compare the constructed measurement circuits, Naimark, hybrid Naimark-QNN, and fully QNN measurements, for strategies of state discrimination, such as minimum-error and maximum-confidence measurements. We demonstrate that QNN circuits can efficiently and effectively achieve near-optimal quantum measurements with fewer training iterations.

I. INTRODUCTION

Measurement readout is an essential building block in quantum information processing. In particular, it is of fundamental interest to construct various forms of a quantum measurement, formulated as a positive-operator-valued measure (POVM), which can be used to reveal nonclassical effects such as hidden quantum nonlocality [1, 2], measurement incompatibility [3], quantum steering [4, 5]. Quantum computing also exploits measurement readout during the computational process. For instance, mid-circuit measurements can provide outcomes that are used to update subsequent qubit operations [6]. Notably, variational quantum algorithms inherently rely on measurements to solve optimization problems [7–11].

Implementations of POVMs can be generally obtained by referring to the Naimark extension [12], see Fig. 1, which realizes a general quantum dynamics by applying a unitary transformation and measuring ancillary qubits. For a state of a system, denoted by $|\psi\rangle$, its general dynamics can be described by a unitary interaction between systems and m ancillary qubits as follows,

$$U_{SA}|\psi\rangle|0\rangle^{\otimes m} = \sum_{i=1}^l [K_i|\psi\rangle] |i\rangle \quad (1)$$

where $\{K_i\}$ denote Kraus operators acting on systems. Measurements on m ancillary qubits in the computational basis $\{|i\rangle\langle i|\}$, where $i = i_1 i_2 \cdots i_m$ for $i_j \in \{0, 1\}$ for $j = 1, \dots, m$, find the probabilities $p(i) = \langle \psi | K_i^\dagger K_i | \psi \rangle$, in which $K_i^\dagger K_i$ constructs a POVM element. Throughout, l -outcome POVM elements, $M = \{M_i\}_{i=1}^l$, can be implemented by the Naimark extension in Eq. (1)

via Kraus operators $\{K_i\}$. We may also include an element M_0 that collects inconclusive outcomes, so that $\sum_{i=0}^l M_i = I$.

Therefore, the complexity of implementing a POVM amounts to the construction of a quantum circuit U_{SA} in Eq. (1), which we call a *measurement circuit*. Recently, a measurement circuit has been presented by following the Naimark extension [13], which can structure a circuit with elementary gates, such as the controlled-NOT (CNOT) and single-qubit gates [14]; hence, arbitrary measurements can be constructed. However, currently available quantum technologies are feasible with shallow-depth quantum circuits, but not with polynomial-depth ones, as full control over quantum errors is yet lacking [15]. It is natural to seek a construction of a measurement circuit such that it may be experimentally feasible and also cost-effective with minimal resources.

Here, we investigate the construction of a circuit ansatz for efficiently composing quantum measurements. The goal is to construct a measurement circuit that may be feasible on the present-day quantum hardware. To this end, we first investigate a measurement circuit for an l -outcome POVM on multiple qubits by following the Naimark extension, framing the circuit in terms of CNOT and single-qubit rotation gates. Then, conversely, we exploit the resulting structured frame as an ansatz on which a classical optimizer can work, and show that the building blocks of a Naimark measurement circuit introduce ZZ-interactions that render the classical search computationally hard.

Then, we address the computational difficulty by replacing the ZZ-interacting building blocks with quan-

tum neural network (QNN) circuits, such as parameterized quantum circuits (PQCs). We present a hybrid Naimark-QNN measurement circuit, in which only the ZZ-interacting blocks are replaced, and show that the number of CNOT gates is significantly reduced compared to the Naimark measurement. We also introduce a fully QNN measurement circuit consisting solely of QNN building blocks, without invoking the Naimark extension.

With measurement-circuit ansatzs, i.e., Naimark, a hybrid Naimark-QNN, and fully QNN measurements, we demonstrate the constructions of measurements in the fundamental task of quantum state discrimination, considering both the minimum-error (ME) and maximum-confidence (MC) strategies. We also present a block-encoding circuit [16, 17] to realize MC measurements. The proof-of-principle demonstrations are performed on a real device, `ibm_strasbourg`, and a simulator, Qiskit Aer. We find that QNN measurement circuits are near-optimal in that they efficiently approximate Naimark measurements, while also being cost-effective: a classical optimizer works more efficiently on QNN measurements than on Naimark ones, and QNN measurements outperform Naimark ones for a smaller number of training iterations. In contrast, a Naimark measurement requires more iterations and ultimately reaches an optimal measurement, whereas its QNN counterpart does not. In Sec. V, we conclude with a summary of the results and remarks on QNN measurements.

This article is structured as follows. In Sec. II, we investigate the Naimark construction of a measurement circuit for l -outcome POVMs of multiple qubits. In Sec. III, we show that building blocks of a Naimark measurement contain two-qubit gates of ZZ-interactions, and replace them with PQCs to construct hybrid Naimark-QNN and fully QNN measurement circuits. In Sec. IV, we demonstrate the construction of measurement circuits for quantum state discrimination, such as ME and MC discrimination. We also present a block-encoding circuit to realize maximum-confidence measurements. In Sec. V, we conclude the results and address remarks on NN measurements.

II. GENERAL MEASUREMENTS BY THE NAIMARK EXTENSION

In this section, we investigate the construction of a general l -outcome measurement on multiple qubits. We generalize the construction in Ref. [13] to multiple qubits to frame the structure of CNOT and single-qubit gates in a Naimark measurement. We present a circuit ansatz for a Naimark measurement; see also related constructions [18–22]. We review the single-qubit POVM in detail and then present a general quantum-

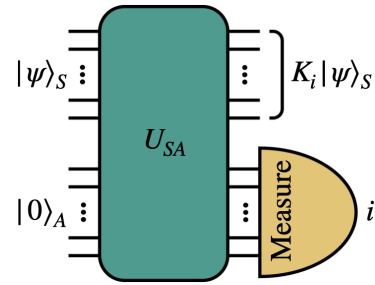


FIG. 1: A general measurement can be implemented in a quantum circuit via the Naimark extension. A circuit U_{SA} over a system and ancilla qubits is performed and an outcome on ancilla qubits, say i (yellow), implements a general operation described by a Kraus operator K_i , where $K_i = {}_A \langle i | U_{SA}$.

circuit architecture for l -outcome measurements, enabling a classical optimizer to find optimal parameters for single-qubit gates.

A. Single-qubit POVM

The strategy of realizing a Naimark measurement on a single-qubit measurement is to sequentially apply two-qubit and single-qubit unitary gates to increase the number of outcomes [13]. To construct a two-outcome measurement, we consider a unitary transformation of a single-qubit state $|\psi\rangle$ as follows,

$$|\psi\rangle|0\rangle \mapsto (V_1 D_1 U)|\psi\rangle|0\rangle + (V_2 D_2 U)|\psi\rangle|1\rangle \quad (2)$$

where U and V_i for $i = 1, 2$ are single-qubit gates and D_i are diagonal ones,

$$\begin{aligned} D_1 &= \cos \theta_1 |0\rangle\langle 0| + \cos \theta_2 |1\rangle\langle 1|, \text{ and} \\ D_2 &= \sin \theta_1 |0\rangle\langle 0| + \sin \theta_2 |1\rangle\langle 1|. \end{aligned} \quad (3)$$

That is, operators $V_i D_i U$ for $i = 1, 2$ on a system S form Kraus operators. They can be explicitly implemented in a circuit as follows,

$$\quad (4)$$

where controlled-Y gates realize rotations on the X-Z plane. Then, a measurement outcome i in the second register realizes a transformation $V_i D_i U$ on a system qubit in the first register.

To generalize the construction above to l -outcome measurements, we need several pieces of machinery as follows. Let us consider an L -bit string $x = x_1 x_2 \cdots x_L$, in which $x_i \in \{0, 1\}$. Let C denote a set of indices

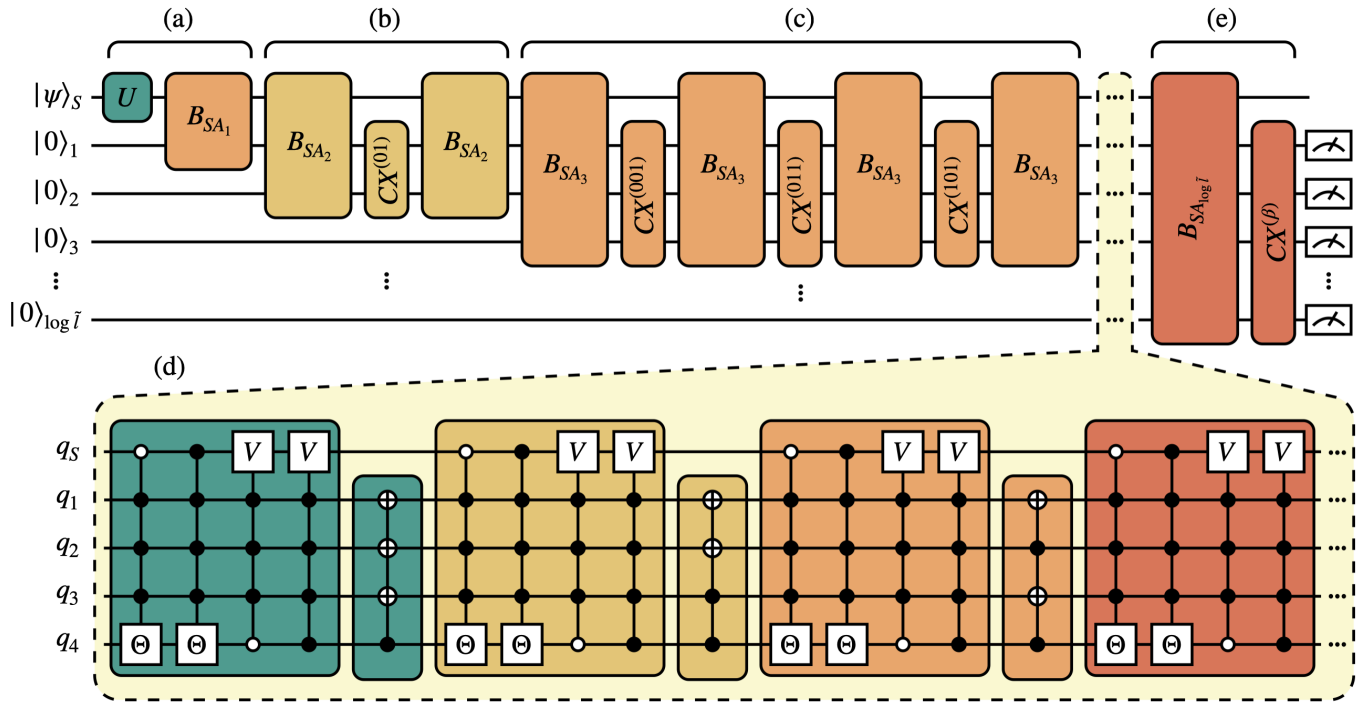


FIG. 2: The construction of a measurement circuit is detailed: l -outcome POVM elements for measurements on $1 + \log_2 \tilde{l}$ qubits are shown by following the Naimark theorem [13, 23] where $\tilde{l} = 2^{\lceil \log_2 l \rceil}$ is the nearest power of 2 not smaller than l . (a) Two-outcome measurements can be prepared after a binary module B_{SA_1} in Eq. (7). (b) After the first B_{SA_2} and $CX^{(01)}$, a three-outcome measurement is realized. To add a POVM element, gate B_{SA_2} is applied, after which four-outcome measurement is achieved. (c) Similarly, a five-outcome measurement is realized after the first B_{SA_3} and $CX^{(001)}$. Then, a POVM can be added after two gates B_{SA_3} and CX . Hence, eight-outcome measurements are realized. (d) A gate B_{SA_4} is composed of CNOT gates and Y -rotation gate parameterized by Θ . (e) shows the final gates: $B_{SA_{\log \tilde{l}}}$ and $CX^{(\beta)}$.

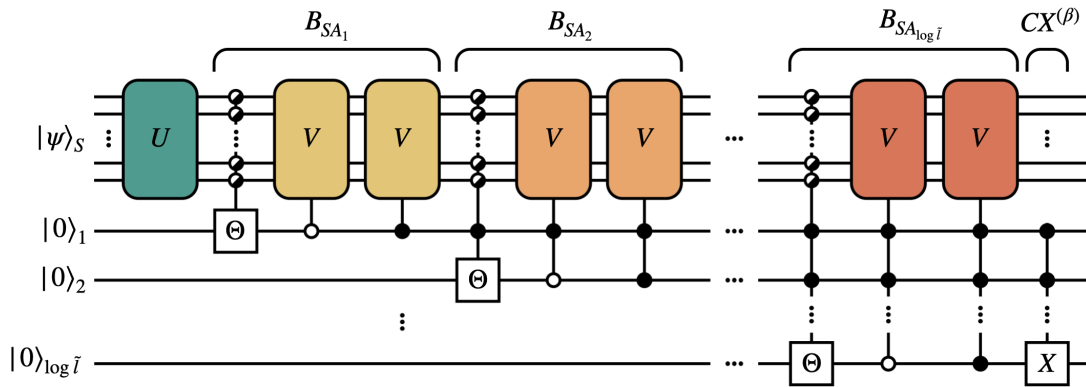


FIG. 3: Multi-qubit POVM extended from the single-qubit case. The single-qubit unitaries U and V are replaced with multi-qubit gates. The two single-qubit R_Y rotations can be interpreted to uniformly controlled rotation gates applied to the given single-qubit state, and thus generalized to uniformly controlled rotations on the prepared multi-qubit state. The $CX^{(x)}$ gates remains unchanged. The overall construction principles of the POVM are preserved. See Fig. 2 for the definitions of \tilde{l} and β .

gate $U \in \mathbf{U}(4)$ can be found by a canonical decomposition [24]

$$U = (A_1 \otimes A_2) \cdot N(\alpha, \beta, \gamma) \cdot (A_3 \otimes A_4), \quad (8)$$

TABLE I: POVM circuit construction.

POVMs	Ancillas	Unitary blocks	Register added
2	1	B_{SA_1}	$ 1\rangle_1$
3	2	$CX^{(01)} B_{SA_2}$	$ 01\rangle_{12}$
4	2	B_{SA_2}	$ 11\rangle_{12}$
5	3	$CX^{(001)} B_{SA_3}$	$ 001\rangle_{123}$
6	3	$CX^{(011)} B_{SA_3}$	$ 011\rangle_{123}$
7	3	$CX^{(101)} B_{SA_3}$	$ 101\rangle_{123}$
8	3	B_{SA_3}	$ 111\rangle_{123}$
9	4	$CX^{(0001)} B_{SA_4}$	$ 0001\rangle_{1234}$
10	4	$CX^{(0011)} B_{SA_4}$	$ 0011\rangle_{1234}$
11	4	$CX^{(0101)} B_{SA_4}$	$ 0101\rangle_{1234}$
12	4	$CX^{(0111)} B_{SA_4}$	$ 0111\rangle_{1234}$
13	4	$CX^{(1001)} B_{SA_4}$	$ 1001\rangle_{1234}$
14	4	$CX^{(1011)} B_{SA_4}$	$ 1011\rangle_{1234}$
15	4	$CX^{(1101)} B_{SA_4}$	$ 1101\rangle_{1234}$
16	4	B_{SA_4}	$ 1111\rangle_{1234}$
17	5	$CX^{(00001)} B_{SA_5}$	$ 00001\rangle_{12345}$

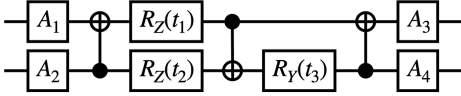


FIG. 4: A two-qubit gate can be generally decomposed by single-qubit rotations and CNOT gates [24]. A canonical construction contains three CNOT gates, single-qubit rotations about Y and Z -axis, and are single-qubit gates $\{A_i\}$.

where $\{A_j \in \mathbf{U}(2)\}$ are single-qubit gates and

$$N(\alpha, \beta, \gamma) = \exp[i(\alpha\sigma_x \otimes \sigma_x + \beta\sigma_y \otimes \sigma_y + \gamma\sigma_z \otimes \sigma_z)],$$

with $\alpha, \beta, \gamma \in \mathbb{R}$. The circuit implementation of $\mathbf{U}(4)$ is shown in Fig 4. Following the strategies shown in the case of a single-qubit POVM, an l -outcome POVM on two-qubit systems can be constructed, see Fig. 3 for a general construction.

C. Classical optimizer and the computational hardness

Having presented a measurement circuit for l -outcome measurements, see also Figs. 2 and 3, one can now conversely exploit it as a circuit ansatz, leaving parameters of single-qubit gates unknown and later to be fixed by a classical optimizer. We observe that what matters in an l -outcome Naimark measurement is the structure of CNOT gates and single-qubit gates in the right places, and a set of parameters of single-qubit gates characterizes an l -outcome measurement. The construction of a measurement circuit is henceforth reduced to searching for optimal parameters of single-qubit gates. To this end, a classical optimizer can be used to construct a measurement circuit universally.

We point out that a Naimark measurement shares the structure with quantum approximate optimization algorithms (QAOAs) for quadratic unconstrained binary optimization (QUBO), which is generally NP-Hard. QAOAs introduce an ansatz iterating a target and a mixing Hamiltonians, H_T and H_M , respectively

$$U(\beta, \gamma) = \prod_{j=1}^p \exp[-i\beta_j H_M] \exp[-i\gamma_j H_T] \quad (9)$$

where the task is to optimize classical parameters $\beta = (\beta_1, \dots, \beta_p)$ and $\gamma = (\gamma_1, \dots, \gamma_p)$ for a p . Note that optimizing a target H_T with two-body interactions is the main challenge, given as an Ising interactions as follows,

$$\exp[-iJ_{12}\gamma_l\sigma_1^{(z)}\sigma_2^{(z)}] = \text{CNOT} \left[R_z(2\gamma_l J_{12}) \right] \text{CNOT} \quad (10)$$

with a coupling parameter J_{12} , where γ_l is a parameter in the l -th layer iteration in QAOAs, see Eq. (9).

Let us revisit a Naimark measurement, see also a circuit in Eq. (4), and find that a controlled rotation is decomposed as follows,

$$\text{CNOT} \left[R_Y(\theta) \right] = \text{CNOT} \left[R_Y(\theta/2) \right] \text{CNOT} \left[R_Y(-\theta/2) \right] \text{CNOT}$$

which contains single-qubit rotations and CNOT gates. Note that we have used the relation $e^{i\phi Y} X = X e^{-i\phi Y}$ and also that Y - and Z -rotations are connected by elementary gates, $R_Y(\theta) = (SH)R_Z(\theta)(SH)^\dagger$ where H is a Hadamard gate and $S = \text{diag}[1, i]$ a phase gate.

Hence, optimizing the parameters of a controlled rotation in a Naimark circuit reproduces, up to a local unitary, the same Ising-type structure that makes QAOA landscapes empirically difficult for local optimizers. This structural similarity suggests that a classical optimizer attempting to fix parameters of a Naimark circuit will face a landscape of local minima and slow convergence, consistent with what is observed numerically in Sec. IV.

III. QUANTUM NEURAL-NET MEASUREMENTS

In this section, we attempt to circumvent the computational hardness of constructing a measurement circuit using a classical optimizer. We introduce QNN circuits as an ansatz for realizing quantum measurements. We, in particular, consider two types of POCs [25] in QNN measurement circuits. One is a hardware-efficient ansatz (HEA), and the other is a circuit block (CB), as shown in Fig. 6. The former is composed of single-qubit rotations followed by nearest-neighbor CNOT gates. The structure leads to shallow quantum circuits and

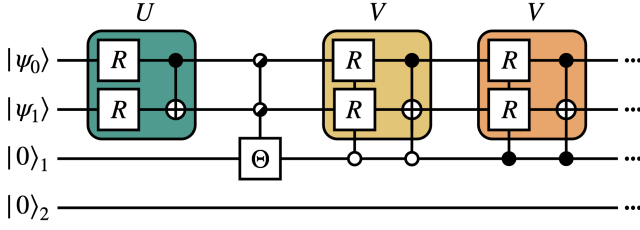
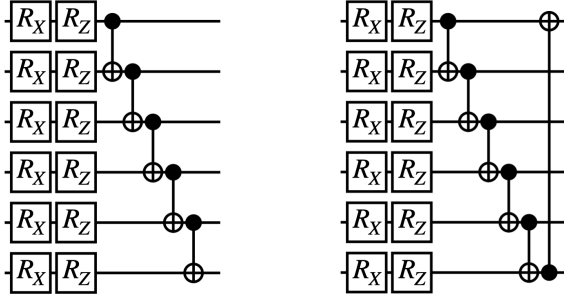


FIG. 5: A hybrid Naimark-QNN measurement for two-qubit states is shown. In a Naimark circuit in Fig. 3, and multi-qubit unitaries on a system are replaced by PQCs. Note that a Naimark and a hybrid Naimark-QNN measurements share the same circuit structure: CNOT gates to include ancillary qubits are placed in the same way.



(a) A HEA unit

(b) A circuit-block (CB)

FIG. 6: Two PQCs are applied as an ansatz for QNN measurements. (a) A hardware-efficient ansatz (HEA) consists of single-qubit gates and nearest-neighbor CNOT gates aligned with hardware connectivity. (b) A circuit-block (CB) unit includes long-range gates that enhance qubit connectivity and expressibility.

aligns with the typical connectivity of superconducting qubits, thereby reducing the likelihood of errors during execution. The latter includes an additional long-range CNOT gate connecting the most distant qubits. The CB exhibits higher expressibility than HEA [25].

A. Hybrid Naimark-quantum-neural-network measurement

We recall that a measurement circuit on n -qubit states is generally $U(2^n)$, which also contains ZZ -interactions that may cause computational costs. We here present hybrid Naimark-QNN quantum measurements by replacing gates $U \in U(2^n)$ with PQCs. We then optimize the parameters of PQCs with a classical optimizer.

Then, a hybrid Naimark-QNN measurement circuit keeps a series of collective CNOT gates, $CX^{(x)}$, that are exploited to include ancillary qubits for having multiple outcomes, while including PQCs in places of uni-

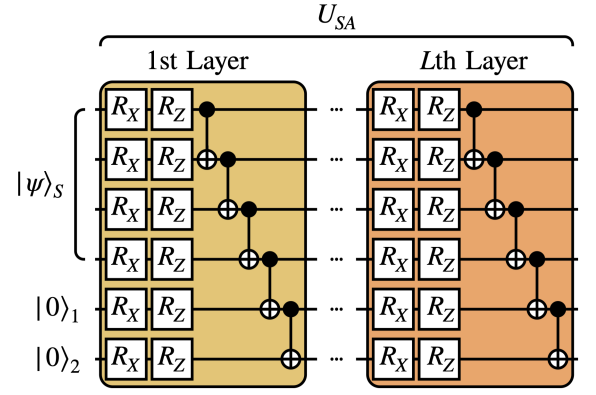


FIG. 7: A fully QNN quantum measurement circuit U_{SA} is shown, where each layer is constructed by HEA. Parameters of single-qubit gates in HEA are optimized. Multiple layers may enhance QNN measurements by increasing expressibility, approximating ideal measurements.

tary circuits on system qubits. In Fig. 5, an instance of hybrid Naimark-QNN measurements with HEA is shown; a two-qubit gate $U(4)$, as shown in Fig. 4, is replaced by HEAs. A classical optimizer is used to find parameters that determine PQCs.

B. Quantum-Neural-network Measurement

We introduce QNN measurement circuits fully by placing PQCs throughout, not keeping the structure of the Naimark measurement, as shown in Fig. 7. Note that a measurement circuit does not contain ZZ -interactions, and the number of CNOT gates increases linearly, so that a classical optimizer may work efficiently. The construction using PQCs is also more favorable for near-term hardware, since it requires fewer CNOT gates. Since PQCs may not form a set of universal gates, multiple PQC layers are used to increase expressibility.

Note that QNN quantum measurements do not explicitly control the number of POVM elements. Let us consider a QNN measurement for l outcomes, and suppose that m ancillary qubits are exploited. Then, overall, 2^m outcomes may be found, whereas $l \leq 2^m$ POVM elements are needed for l outcomes.

In Fig. 7, a QNN measurement for a four-qubit system with two ancillary qubits is shown with HEA. L layers are applied to approximate an optimal measurement.

IV. CONSTRUCTING MEASUREMENT CIRCUITS FOR STATE DISCRIMINATION

We here apply the constructions of measurement circuits to optimal quantum state discrimination, a fundamental task of a quantum measurement. We consider strategies of ME [26–29] and MC discrimination [30]. Note that MC discrimination is more general than unambiguous discrimination [28] since it coincides with unambiguous state discrimination [31] for linearly independent states [32].

As for the proof-of-principle demonstrations, we consider two sets of states. The first instance is a set of three states given with equal *a priori* probabilities [33],

$$\text{Ensemble 1: } S_1 = \{|\psi_i\rangle\}_{i=0}^2 \text{ where} \quad (11)$$

$$|\psi_0\rangle = |0\rangle, \quad |\psi_1\rangle = \sqrt{\frac{2}{3}}|0\rangle + \sqrt{\frac{1}{3}}|1\rangle,$$

$$\text{and } |\psi_2\rangle = \sqrt{\frac{2}{3}}|0\rangle - \sqrt{\frac{1}{3}}|1\rangle.$$

The other instance is with multiple-qubit states, copies of trine states [34],

$$\text{Ensemble 2: } S_2 = \{|\psi_i\rangle = |a_i\rangle^{\otimes n}\}_{i=0}^2 \text{ where} \quad (12)$$

$$|a_0\rangle = |0\rangle, \quad |a_1\rangle = \frac{1}{2}|0\rangle + \frac{\sqrt{3}}{2}|1\rangle,$$

$$\text{and } |a_2\rangle = \frac{1}{2}|0\rangle - \frac{\sqrt{3}}{2}|1\rangle.$$

An ensemble above can be prepared with a circuit U_{PREP} such that

$$U_{\text{PREP}}|0\rangle_P^{\otimes \lceil \log_2 n \rceil} |0\rangle_S^{\otimes n} = \sum_{k=0}^{l-1} \sqrt{q_k} |k\rangle_P |\psi_k\rangle_S \quad (13)$$

and measuring the ancillary qubits of register P , where q_k is *a priori* probability for a state $|\psi_k\rangle$. In what follows, we construct measurement circuits with a classical optimizer.

A. Measurement for minimizing average errors

In ME discrimination, a measurement attempts to provide a guess, with minimal average error, about which state has been prepared. The guessing probability is given by,

$$p_{\text{guess}} = \max_{M_i} \sum_i p_i \text{tr}[M_i \rho_i]. \quad (14)$$

where $\{M_i\}$ forms a complete measurement. We construct a measurement in three approaches.

- *Naimark measurements with a classical optimizer.* Firstly, we exploit the structure of an Naimark

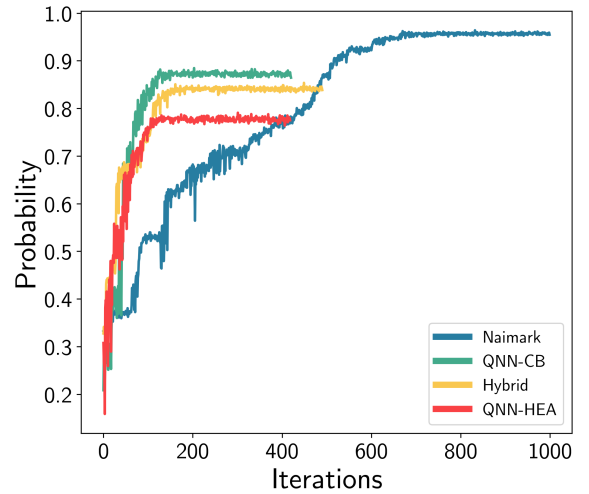


FIG. 8: (a) Measurements are constructed by a classical optimizer for ME discrimination of an ensemble of two-copy states in Eq. (12), i.e., S_2 with $n = 2$. The optimization of a Naimark measurement circuit is relatively inefficient, as a larger number of iterations is needed to reach the ultimate guessing probability. A fully QNN measurement circuit with CB blocks (green), a hybrid Naimark-QNN measurement circuit (yellow), and a fully QNN measurement circuit with HEA (red) are constructed by a classical optimizer. QNN measurements do not reach the highest value of the guessing probability although they are efficiently optimized for a smaller number of iterations.

measurement as shown in Figs. 2 and 3. In the construction, we leave single-qubit gates with parameters to be fixed, which are then trained on the circuit with a classical optimizer to find optimal parameters. Once a set of parameters is fixed, we have a measurement for ME discrimination.

- *hybrid Naimark-QNN measurements with a classical optimizer.* Secondly, we keep the structure of Naimark measurements and apply QNN circuits on system qubits, which we call hybrid Naimark-QNN measurements. For the ensemble S_2 in Eq. (12), we replace two-qubit exact gates in $U(4)$ with PQCs and apply a classical optimizer.
- *Fully QNN measurements with a classical optimizer.* Thirdly, we attempt to construct POVMs with QNN measurements in Fig. 7 for ensembles S_1 and S_2 by using a classical optimizer.

Resources: CNOT gates

CNOT gates in QNN measurements increase linearly in the number of qubits. In contrast to QNN cases, a

Naimark measurement circuit requires an even larger number of CNOT gates. Consider an l -outcome POVM for n -state discrimination. Note that the number of outcomes, denoted by l , is related to the number of ancillary qubits n_A . Let us summarize the resources needed in terms of the number of CNOT gates, which are the main challenge in the currently available quantum technologies.

For a Naimark measurement circuit constructed here, the number of CNOT gates required is given by $O(2^n l^2)$. Implementation of l outcomes requires $n_A = \lceil \log_2 l \rceil$ ancillary qubits, where $l \in (2^{n_A-1}, 2^{n_A}]$. The count is derived in detail in the Appendix. When n_A is dominant, i.e., a larger number of outcomes is needed, the overall number of CNOT gates increases rapidly.

Let us also compare the count with a Naimark measurement circuit presented in Ref. [35], where the number of CNOT gates is given by $O(2^{2n} l)$ with $l = 2^{n_A}$. The number increases rapidly as a system contains more qubits; however, the overall count is less dependent on ancillary qubits.

It is worth mentioning that ME discrimination of n -qubit states does not have to contain more than $(2^n)^2$ outcomes to achieve the guessing probability in general, even if the number of states l is larger than $(2^n)^2$ [36]. For instance, one does not need to have more than 4 outcomes in ME discrimination of l qubit states for arbitrary $l \geq 2$. Hence, one can restrict $n_A \leq 2n$ without loss of generality.

Demonstration

We optimize measurement circuits constructed in the three approaches above to find the guessing probability in Eq. (14). We consider ensembles S_1 and S_2 in Eqs. (11) and (12), and apply COBYLA as a classical optimizer. Ensemble S_1 is a collection of single-qubit states, and S_2 contains n -copy states. We increase the number of copies up to $n = 3$, above which it is not feasible to optimize a Naimark measurement circuit having universal gates.

We consider optimal discrimination for an ensemble of two-copy states S_2 in Eq. (12), i.e., for $n = 2$, and attempt to construct measurement circuits with a classical optimizer. In Fig. 8, we demonstrate the convergence of guessing probabilities along the three approaches. One can observe that a classical optimizer is less efficient in working in a Naimark measurement circuit than QNN ones. For a smaller number of iterations, QNN circuits are efficiently optimized. With a Naimark measurement circuit, a classical optimizer eventually constructs an optimal measurement. However, QNN measurement circuits ultimately do not reach the guessing probability of an optimal measurement. We conclude that a

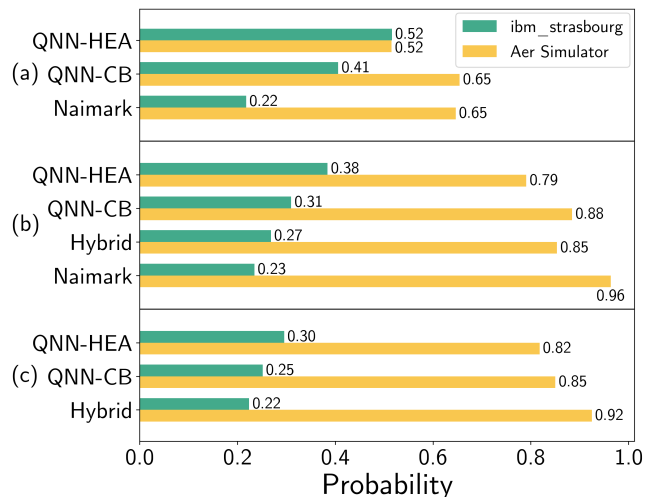


FIG. 9: Naimark and QNN measurement circuits for optimal quantum state discrimination are constructed for ensembles S_1 and S_2 in Eqs. (11) and (12), respectively. They are demonstrated in a real hardware `ibm_strasbourg` (green) and in a simulator Qiskit Aer (yellow). We have collected data from `ibm_strasbourg` on 29/11/2024. (a) Naimark and QNN measurement circuits are constructed for an ensemble S_1 , and (b) an ensemble of two-copy states S_2 for $n = 2$. (c) QNN measurements are realized for three-copy states of S_3 , i.e., $n = 3$, for which the construction of a Naimark measurement circuit has a high depth and a classical optimizer does not work for the construction. In all instances, a classical optimizer is the most efficient for constructing QNN measurement circuits with HEA and the least efficient for Naimark measurement circuits.

Naimark measurement circuit is inefficiently optimized but ultimately converges to an optimal one, whereas the QNN constructions are efficiently optimized, though they do not reach the optimal value of the figure of merit.

We then consider measurement circuits for optimal discrimination for ensembles S_1 and S_2 with `ibm_strasbourg`; data were collected on 29/11/2024. We have also run the circuits with a simulator Qiskit Aer for comparing optimization tasks on noisy and noiseless devices. For ensemble S_2 , we compute ME discrimination of two- and three-copy states.

In Fig. 9, the result of optimizing measurement circuits is summarized. It is demonstrated that QNN measurement circuits with HEA are the most favorable for an optimizer to work with a real and noisy quantum hardware. The second favorable one is also a QNN measurement with CB. The next one is fraction QNN measurements, which keep the structure of the Naimark extension. It turns out to be a Naimark measurement circuit in which optimizing parameters is

the most difficult. The caveat is that, even in a noiseless scenario, it becomes highly inefficient to optimize a Naimark measurement on multiple qubits.

We observe that the key distinction lies in the distribution of CNOT gates in a circuit. Both a fraction QNN and a Naimark measurement share an identical arrangement of CNOT gates, where CNOT gates are not sequential between qubits: CNOT operations over qubits far in distance are also required. Fully QNN measurements with HEA contain CNOT gates between nearest qubits; CB includes a single CNOT over two qubits that are not nearest neighbors with each other.

B. Maximum confidence measurement

We consider a maximum-confidence (MC) measurement that generalizes strategies for state discrimination [28, 30]. For an ensemble $\{q_i, \rho_i\}$, i.e., a state ρ_i appears with a probability q_i , suppose that an outcome k occurs, which makes a guess a state ρ_k . An MC measurement introduces the notion of confidence in a detection event, namely, by defining the probability that the guess is correct as the confidence on a detection event. The confidence is thus defined as a conditional probability,

$$C(k) = P_{P|M}(k|k) = \frac{p_P(k) p_{M|P}(k|k)}{p_M(k)}$$

where P and M denote preparation and a measurement, respectively. Since we have $p_P(k) = q_k$, $p_{M|P}(k|k) = \text{tr}[\rho_k M_k]$ and $p_M(k) = \text{tr}[\rho M_k]$, where $\rho = \sum_i q_i \rho_i$, the maximum confidence is given by

$$\max C(i) = \max_{M_i} \frac{q_i \text{tr}[\rho_i M_i]}{\text{tr}[\rho M_i]} \quad (15)$$

which asks an optimization of a POVM element. Note that the optimization problem has been analytically solved for qubit states [37] and is generally approached by a semidefinite program [38].

The optimization problem can be facilitated by taking an ansatz $M_i = c_i \rho^{-\frac{1}{2}} Q_i \rho^{-\frac{1}{2}}$ for some $Q_i \geq 0$ and constant c_i so that the problem becomes linear

$$C(i) = \max_{Q_i \geq 0, \text{Tr}[Q_i]=1} \text{tr}[\rho^{-\frac{1}{2}} q_i \rho_i \rho^{-\frac{1}{2}} Q_i]. \quad (16)$$

Note that it suffices to consider a rank-one projector in the maximization, which simplifies the problem to find a unitary circuit U such that $Q_i = U|i\rangle\langle i|U^\dagger$. After all, we can formulate MCMs for an ensemble $\{q_i, \rho_i\}$ as follows,

$$\max_U \text{tr}[U^\dagger \rho^{-\frac{1}{2}} q_i \rho_i \rho^{-\frac{1}{2}} U|i\rangle\langle i|]. \quad (17)$$

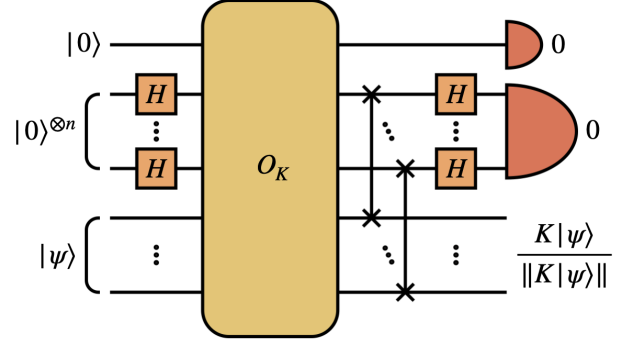


FIG. 10: The block-encoding method is shown for the realization of Eq. (18). A Kraus operator K is realized on system qubits when measurement outcomes in the ancillary qubits are all zeros.

Therefore, we arrive at the problem of constructing a unitary circuit U for an ensemble.

The optimization problem in Eq. (17) contains two steps: firstly, we realize a projection onto the subspace spanned by $\sqrt{\rho}^{-1}$, and secondly, after the projection is successful, we optimize a unitary circuit U . The former corresponds to a state filtration by a Kraus operator proportional to $\sqrt{\rho}^{-1}$, and can be realized by a block-encoding (BE), and the latter by a classical optimizer.

We write by U_{BE} for the purpose, as follows,

$$U_{BE} \left[\sum_{k=0}^{l-1} \sqrt{q_k} |k\rangle_{A_1} |\psi_k\rangle_S \otimes |0\rangle_{A_2}^{\otimes n+1} \right] \\ = \sum_{k=0}^{l-1} \sqrt{q_k} |k\rangle_{A_1} K |\psi_k\rangle_S \otimes |0\rangle_{A_2}^{\otimes n+1} + |\Phi^\perp\rangle \quad (18)$$

where A_1 denote ancillary qubits for preparing an ensemble $\{q_k, |\psi_k\rangle\langle\psi_k|\}$, $|\Phi^\perp\rangle$ is given such that $A_2 \langle 0|^{\otimes n+1} |\Phi^\perp\rangle = 0$, and

$$K = \frac{1}{c} \rho^{-1/2} \text{ where } c = 2^n \max_{ij} |(\rho^{-1/2})_{ij}|.$$

Note that $K^\dagger K \leq I$ for the construction above since we have $\|K\|_2^2 \leq \|K\|_1 \|K\|_\infty$ in which $\|K\|_1, \|K\|_\infty \leq 1$ given $K = [K_{ij}]$ where $|K_{ij}| \leq 1/2^n$. Measurement outcomes $0^{\times(n+1)}$ in ancillary qubits of the register A_2 realizes a transformation $\rho^{-1/2}$ on system qubits, see Eq. (17). In the following, we summarize strategies for block-encoding and unitary optimization.

Block-encoding

To implement a block-encoding K , we employ the method shown in Ref. [40], see Fig. 10. Let U_K denote a

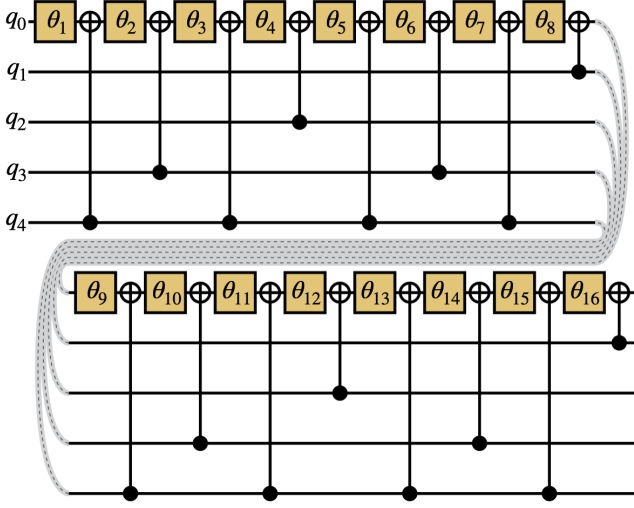


FIG. 11: A unitary transformation O_K in the block-encoding in Fig. 10 is shown for system qubits q_3 and q_4 with ancillary qubits q_0, q_1 and q_2 . A Gray code [39] applies to qubits in registers $q_1 q_2 q_3 q_4$ and CNOT gates are placed between q_0 and q_i for $i \in \{1, 2, 3, 4\}$. For instance, starting from the Gray code 0000, a CNOT gate is placed between q_0 and q_3 for a code 0011.

unitary circuit for the block-encoding that implements an n -qubit Kraus operator K

$$K = \left(|0\rangle^{\otimes n+1} \otimes I_n \right) U_K \left(|0\rangle^{\otimes n+1} \otimes I_n \right) \quad (19)$$

where U_K contains Hadamard and SWAP gates as well as a $(2n + 1)$ -gate O_K that works as follows

$$O_K |0\rangle |i\rangle |j\rangle = \left(2^n K_{ij} |0\rangle + \sqrt{1 - 4^n K_{ij}^2} |1\rangle \right) |i\rangle |j\rangle$$

for n -qubit states $|i\rangle$ and $|j\rangle$. One can implement O_K by using $2^n \times 2^n$ controlled- R_Y gates,

$$O_K = \sum_{i, j=1}^{2^n} R_y(2\theta_{ij}) \otimes |i\rangle \langle i| \otimes |j\rangle \langle j|$$

where $\theta_{ij} = \arccos(2^n K_{ij})$. One can construct O_K with CNOTs and single-qubit gates, see Fig. 11. A circuit implementation of O_K may introduce another parameterization, denoted by $\hat{\theta}$, where we apply a cutoff condition that small rotations below a threshold, i.e., $\hat{\theta}_{ij} \leq \delta_c$, are ignored. We write by \tilde{K} the Kraus operator resulting from the final circuit implementation, including the cut-off constraint, and the approximation can be estimated by the cutoff parameter, $\|K - \tilde{K}\|_2 \leq 4^n \delta_c$ [40].

Optimizing a unitary circuit

After block-encoding is successfully realized, the next step is to optimize a unitary circuit for an MC measure-

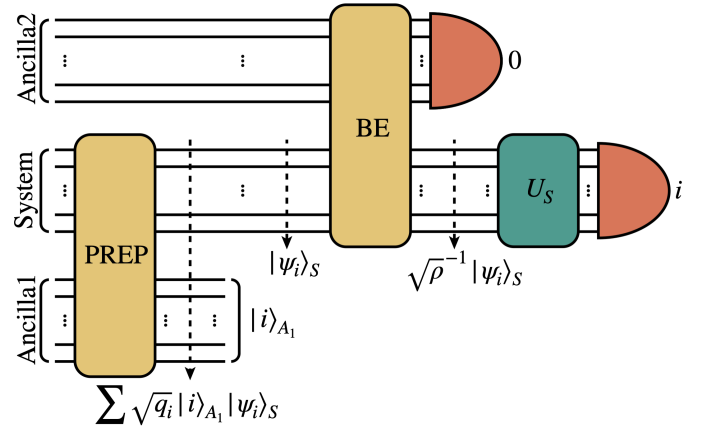


FIG. 12: The circuit of the proof-of-demonstrations of MC discrimination is summarized. An ensemble is prepared by a unitary circuit PREP; measurement i occurs with *a priori* probability q_i , and prepares a state $|\psi_i\rangle$ on system qubits. A circuit BE realizes a block-encoding that implements a projection $\rho^{-1/2}$; a measurement outcome 0 concludes a successful realization of the projection on systems qubits. Once a block encoding is applied, a unitary circuit U_S is optimized to maximize the confidence values.

ment, i.e., U in Eq. (17). A circuit for the optimization generally requires universal gates such as single-qubit rotations and CNOT gates, where we call an exact construction a Naimark measurement, in a manner similar to ME discrimination. Note that the exact construction coincides with measurements for ME discrimination when an MCM is constrained to have no inconclusive measurement outcomes.

Let $U := U(\Theta)$ denote a circuit with a set of parameters Θ , either universal or QNN measurement circuits. Firstly, one can consider optimizing parameters for universal gates and may ultimately achieve the highest MC values. Secondly, one can efficiently exploit a classical optimizer by relaxing a circuit with universal gates with QNN measurement circuits. Similar to cases of ME discrimination, we exploit fully QNN measurement circuits with HEA and CB.

Demonstration

We consider MC discrimination for ensembles in Eqs. (11) and (12). For each ensemble, we first implement the FABLE for block-encoding, and then optimize a unitary gate $U(\Theta)$ by Naimark or QNN measurement circuits. For block-encoding, we ignore single-qubit gates having sufficiently small angles $\theta_{ij} \leq \delta_c$ for efficient realizations. Discarding small-angle rotations introduces errors in the approximation: we take a cut-off

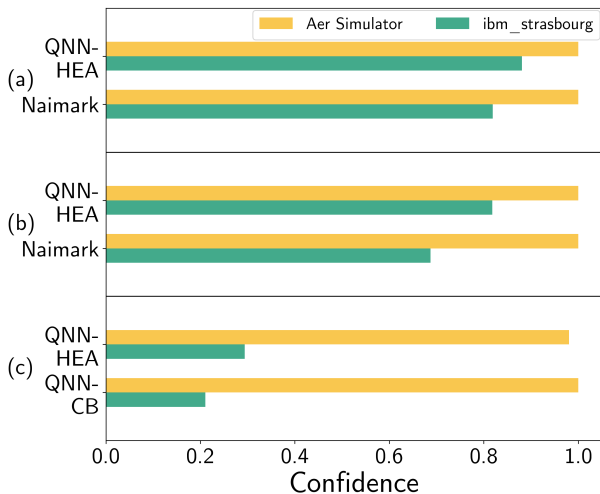


FIG. 13: The construction of measurement circuits for MC discrimination is demonstrated in a real and noisy hardware, `ibm_strasbourg` (green), and a simulator, Qiskit Aer (yellow). Fully QNN with HEA and Naimark measurement circuits are constructed for MC measurements of ensemble (a) S_1 in Eq. (11), and (b) S_2 in Eq. (12) of two-copy states, i.e., $n = 2$. (c) For the ensemble S_2 of three-copy states, i.e., $n = 3$, fully QNN measurements are considered with HEA and CB, respectively. In all cases with realistic noisy devices, fully QNN measurement circuits with HEA and a classical optimizer achieve the highest confidence values. From instance (c), HEA is also more favorable than CB when constructing MC measurements on noisy quantum hardware.

$\delta_c = 0.005$ 1 and 2-qubit cases to maintain the accuracy. In the 3-qubit case, due to the significant circuit depth caused by serial application of $2^n \times 2^n$ CNOT gates, we have to set a slightly larger threshold $\delta_c = 0.025$.

To optimize a unitary circuit with a classical optimizer, we exploit a Naimark and QNN measurement circuits. QNN measurement circuits may apply HEA or CB structures. Proof-of-principle demonstrations are conducted on a realistic, noisy device, `ibm_strasbourg`, for which data were collected on 24/11/2024, and also in the Qiskit Aer Simulator.

The results are summarized in Fig. 13. A classical optimizer attempts to find optimal parameters of a Naimark measurement and fully QNN measurements with HEA or CB. Although a Naimark measurement can ultimately reach the highest confidence values, it does not achieve the confidence values on noisy quantum devices. QNN measurements with HEA, which will not construct optimal MC measurements, turn out to be effective on noisy quantum hardware. They even outperform CB for an ensemble of three-copy states.

V. CONCLUSION

In conclusion, we have investigated quantum measurements within the circuit model. We have constructed l -outcome Naimark measurements using universal gates: CNOTs together with single-qubit rotations that can, in principle, realize arbitrary POVMs. We have shown that Naimark measurement circuits share a structural correspondence with quantum algorithms for QUBO problems, which are computationally hard. This observation suggests that a Naimark circuit is unlikely to serve as a useful ansatz for quantum optimization. As an alternative, we have introduced QNN measurement circuits based on the hardware-efficient ansatz or the checkerboard layout, both of which are better suited to realistic, noisy quantum hardware: the number of CNOT gates scales linearly with system size, and entangling operations act only on neighboring qubits sequentially.

We have applied these constructions to two canonical problems in optimal quantum state discrimination: minimizing the average error probability, and maximizing the confidence of measurement outcomes. For minimum-error measurements, we have introduced a hybrid QNN scheme that retains the overall structure of a Naimark measurement while replacing the m -qubit universal circuit $U(m)$ with a QNN circuit. For maximum-confidence measurements, we have devised a block-encoding circuit and employed QNN circuits to optimize the corresponding unitary operations.

Proof-of-principle demonstrations of both ME and MC measurements were performed on the noisy superconducting device `ibm_strasbourg` and on the Qiskit Aer simulator. In all cases, we find that classical optimization is most efficient for QNN measurements with HEA: the circuits converge within a relatively small number of training iterations. Classical optimization is markedly less efficient for Naimark measurements, which require substantially more iterations to converge. On the other hand, Naimark measurements can, in principle, attain the optimal measurement exactly, whereas QNN measurements generally cannot. A clear trade-off therefore emerges between optimization efficiency and the precision with which the optimal measurement is approximated. We further note that QNN measurements are particularly well-suited to present-day quantum devices for two reasons: (i) they are efficiently optimized, and (ii) their CNOT gates respect the nearest-neighbor connectivity of typical qubit arrays.

It remains an open question how to design quantum measurement circuits that are simultaneously efficient to optimize and capable of high-precision approximation on realistic, noisy hardware. A further direction of interest is the treatment of errors specific to mea-

surement circuits, in which the measurement operation itself is intrinsically noisy.

ACKNOWLEDGEMENTS

SWY and JB were supported by the National Research Foundation of Korea (RS-2024-00408613) and the Institute for Information & Communication Technology Promotion (IITP) (RS-2023-00229524, RS-2025-02304540, RS-2025-25464876, RS-2025-25464616). THK was supported by LG Electronics. THK extends thanks to Kevin Ferreira, Yipeng Ji, and Paria Nejat of the LG Electronics Toronto AI Lab and to Sean Kim of LG Electronics, AI Lab, for their support during this research.

-
- [1] S. Popescu, Bell’s inequalities and density matrices: Revealing “hidden” nonlocality, *Phys. Rev. Lett.* **74**, 2619 (1995).
- [2] F. Hirsch, M. T. Quintino, J. Bowles, and N. Brunner, Genuine hidden quantum nonlocality, *Phys. Rev. Lett.* **111**, 160402 (2013).
- [3] T. Heinosaari, T. Miyadera, and M. Ziman, An invitation to quantum incompatibility, *Journal of Physics A: Mathematical and Theoretical* **49**, 123001 (2016).
- [4] H. M. Wiseman, S. J. Jones, and A. C. Doherty, Steering, entanglement, nonlocality, and the einstein-podolsky-rosen paradox, *Phys. Rev. Lett.* **98**, 140402 (2007).
- [5] R. Uola, A. C. S. Costa, H. C. Nguyen, and O. Gühne, Quantum steering, *Rev. Mod. Phys.* **92**, 015001 (2020).
- [6] K. Rudinger, G. J. Ribeill, L. C. Govia, M. Ware, E. Nielsen, K. Young, T. A. Ohki, R. Blume-Kohout, and T. Proctor, Characterizing midcircuit measurements on a superconducting qubit using gate set tomography, *Phys. Rev. Appl.* **17**, 014014 (2022).
- [7] K. Bharti, A. Cervera-Lierta, T. H. Kyaw, T. Haug, S. Alperin-Lea, A. Anand, M. Degroote, H. Heimonen, J. S. Kottmann, T. Menke, W.-K. Mok, S. Sim, L.-C. Kwek, and A. Aspuru-Guzik, Noisy intermediate-scale quantum algorithms, *Rev. Mod. Phys.* **94**, 015004 (2022).
- [8] M. Cerezo, A. Arrasmith, R. Babbush, S. C. Benjamin, S. Endo, K. Fujii, J. R. McClean, K. Mitarai, X. Yuan, L. Cincio, and P. J. Coles, Variational quantum algorithms, *Nature Reviews Physics* **3**, 625 (2021).
- [9] K. Blekos, D. Brand, A. Ceschini, C.-H. Chou, R.-H. Li, K. Pandya, and A. Summer, A review on quantum approximate optimization algorithm and its variants, *Physics Reports* **1068**, 1 (2024), a review on Quantum Approximate Optimization Algorithm and its variants.
- [10] M. Weber, A. Anand, A. Cervera-Lierta, J. S. Kottmann, T. H. Kyaw, B. Li, A. Aspuru-Guzik, C. Zhang, and Z. Zhao, Toward reliability in the nisq era: Robust interval guarantee for quantum measurements on approximate states, *Phys. Rev. Res.* **4** (2022).
- [11] T. H. Kyaw, M. B. Soley, B. Allen, P. Bergold, C. Sun, V. S. Batista, and A. Aspuru-Guzik, Boosting quantum amplitude exponentially in variational quantum algorithms, *Quantum Sci. Technol.* **9**, 01LT01 (2023).
- [12] M. A. Naimark, On a representation of additive operator set functions, *Comptes Rendus (Doklady) de l’Académie des Sciences de l’URSS* **41**, 359 (1943).
- [13] Y. S. Yordanov and C. H. W. Barnes, Implementation of a general single-qubit positive operator-valued measure on a circuit-based quantum computer, *Physical Review A* **100**, 10.1103/physreva.100.062317 (2019).
- [14] A. Barenco, C. H. Bennett, R. Cleve, D. P. DiVincenzo, N. Margolus, P. Shor, T. Sleator, J. A. Smolin, and H. Weinfurter, Elementary gates for quantum computation, *Phys. Rev. A* **52**, 3457 (1995).
- [15] J. Preskill, Quantum Computing in the NISQ era and beyond, *Quantum* **2**, 79 (2018).
- [16] D. Camps and R. Van Beeumen, Fable: Fast approximate quantum circuits for block-encodings, in *2022 IEEE International Conference on Quantum Computing and Engineering (QCE)* (IEEE, 2022) pp. 104–113.
- [17] G. H. Low and I. L. Chuang, Optimal hamiltonian simulation by quantum signal processing, *Phys. Rev. Lett.* **118**, 10.1103/physrevlett.118.010501 (2017).
- [18] E. Andersson and D. K. L. Oi, Binary search trees for generalized measurements, *Phys. Rev. A* **77**, 052104 (2008).
- [19] M. Oszmaniec, L. Guerini, P. Wittek, and A. Acín, Simulating positive-operator-valued measures with projective measurements, *Phys. Rev. Lett.* **119**, 190501 (2017).
- [20] M. Oszmaniec, F. B. Maciejewski, and Z. Puchała, Simulating all quantum measurements using only projective measurements and postselection, *Phys. Rev. A* **100**, 012351 (2019).
- [21] T. Singal, F. B. Maciejewski, and M. Oszmaniec, Implementation of quantum measurements using classical resources and only a single ancillary qubit, *npj Quantum Information* **8**, 82 (2022).
- [22] D. Reitzner and J. Bouda, General measurements with limited resources and their application to quantum unambiguous state discrimination, *Quantum Information Processing* **23**, 268 (2024).
- [23] A. Peres, Neumark’s theorem and quantum inseparability, *Foundations of Physics* **20**, 1441 (1990).
- [24] F. Vatan and C. Williams, Optimal quantum circuits for general two-qubit gates, *Phys. Rev. A* **69**, 032315 (2004).
- [25] S. Sim, P. D. Johnson, and A. Aspuru-Guzik, Expressibility and entangling capability of parameterized quantum circuits for hybrid quantum-classical algorithms, *Adv. Quantum Technologies* **2** (2019).
- [26] C. W. Helstrom, Quantum detection and estimation theory, *Journal of Statistical Physics* **1**, 231 (1969).

- [27] J. A. Bergou, Discrimination of quantum states, *Journal of Modern Optics* **57**, 160 (2010).
- [28] S. M. Barnett and S. Croke, Quantum state discrimination, *Advances in Optics and Photonics* **1**, 238 (2009).
- [29] J. Bae and L.-C. Kwek, Quantum state discrimination and its applications, *Journal of Physics A: Mathematical and Theoretical* **48**, 083001 (2015).
- [30] S. Croke, E. Andersson, S. M. Barnett, C. R. Gilson, and J. Jeffers, Maximum confidence quantum measurements, *Physical Review Letters* **96**, 10.1103/physrevlett.96.070401 (2006).
- [31] D. Dieks, Overlap and distinguishability of quantum states, *Physics Letters A* **126**, 303 (1988).
- [32] H. Lee, K. Flatt, and J. Bae, Sequential quantum maximum-confidence discrimination, *Phys. Rev. A* **112**, 052206 (2025).
- [33] J. Bae, Structure of minimum-error quantum state discrimination, *New Journal of Physics* **15**, 073037 (2013).
- [34] W. K. Wootters, Distinguishing unentangled states with an unentangled measurement, *International Journal of Quantum Information* **4**, 219 (2006).
- [35] D. Lee, K. Baek, J. Huh, and D. K. Park, Variational quantum state discriminator for supervised machine learning (2023), [arXiv:2303.03588 \[quant-ph\]](https://arxiv.org/abs/2303.03588).
- [36] E. Davies, Information and quantum measurement, *IEEE Transactions on Information Theory* **24**, 596 (1978).
- [37] H. Lee, K. Flatt, C. R. i Carceller, J. B. Brask, and J. Bae, Maximum-confidence measurement for qubit states, *Physical Review A* **106** (2022).
- [38] K. Flatt, H. Lee, C. R. I. Carceller, J. B. Brask, and J. Bae, Contextual advantages and certification for maximum-confidence discrimination, *PRX Quantum* **3**, 030337 (2022).
- [39] N. P. D. Sawaya, T. Menke, T. H. Kyaw, S. Johri, A. Aspuru-Guzik, and G. G. Guerreschi, Resource-efficient digital quantum simulation of d-level systems for photonic, vibrational, and spin-s hamiltonians, *npj Quantum Inf.* **6** (2020).
- [40] D. Camps and R. Van Beeumen, Fable: Fast approximate quantum circuits for block-encodings, in *2022 IEEE International Conference on Quantum Computing and Engineering (QCE)* (2022) pp. 104–113.
- [41] V. V. Shende and I. L. Markov, On the cnot-cost of toffoli gates, *Quantum Info. Comput.* **9**, 461 (2009).
- [42] M. Möttönen, J. J. Vartiainen, V. Bergholm, and M. M. Salomaa, Quantum circuits for general multiqubit gates, *Phys. Rev. Lett.* **93**, 130502 (2004).

Appendix A: Types of the $CX^{(x)}$

In this section, we describe the types of $CX^{(x)}$ gates required for Naimark measurement circuit acting on m qubits. We first define the gate MCX_k^l , which denotes a multi-controlled multi-target X gate acting on l target qubits with k control qubits, assuming the last qubit is a control qubit. Hereafter, we use “MCX” generically to refer to a multi-controlled multi-target X gate.

In general, the $CX^{(x)}$ gate is a MCX gate that maps the register $|1\rangle^{\otimes m}$ to $|x\rangle$. In the Naimark measurement circuit, the bitstrings $\{x\}$ used for the $CX^{(x)}$ gates are elements of the set $A(m)$ (see the definition of $A(L)$ in Section II A). The $CX^{(x)}$ should be applied in increasing order of x , as described in the main text. This ordering is obtained by selecting gates sequentially from left to right among the MCX_k^m (from $k = m - 1$ to 1), as shown in Fig. 14. Given the m -bit string $x = x_1x_2 \cdots x_m$, $x_j = 0$ corresponds to applying an X gate to qubit q_j whereas $x_j = 1$ corresponds to using q_j as a control qubit in the MCX gate.

Note that if the $CX^{(x)}$ gates must be applied sequentially across different MCX_k^m gates, although arbitrary ordering within a single MCX_k^m gate is allowed. Otherwise, swaps occur among the pre-existing ancillary registers by B_{SA} gates. In total, there are $2^{m-1} - 1$ such $CX^{(x)}$ gates for m ancillary qubits.

Appendix B: CNOT Count in Multi-qubit POVM Circuit

In this section, we derive the total number of CNOTs, $\mathcal{O}(2^n l^2)$, required for the hybrid Naimark-QNN measurement circuit, as shown in Fig. 5.

1. CNOT Count in the i -th $CX^{(x)}$

We analyze the CNOT count required to implement the i -th $CX^{(x)}$ gate. Both the i -th B_{SA} gate and subsequent $CX^{(x)}$ gate act on $\lfloor \log_2 i \rfloor + 1$ ancillary qubits. Here, the i -th $CX^{(x)}$ gate denotes the one applied immediately after the i -th B_{SA} gate.

Assume that the bitstring x contains k bits equal to 0, corresponding to k X gates applied to the corresponding qubits. The $CX^{(x)}$ has $\lfloor \log_2 i \rfloor + 1 - k$ control qubits. Using the decomposition scheme described in Fig. 15, the gate is decomposed into k multi-controlled X gates, each having $\lfloor \log_2 i \rfloor + 1 - k$ control qubits. According to Ref. [14], a multi-controlled X gate with m control qubits (for $m \geq 5$) can be decomposed into $8(m - 3)$ three-qubit Toffoli gates. Each three-qubit Toffoli can, in turn, be decomposed into 6 CNOT gates [41]. Thus, the multi-controlled X gate with m control qubits can

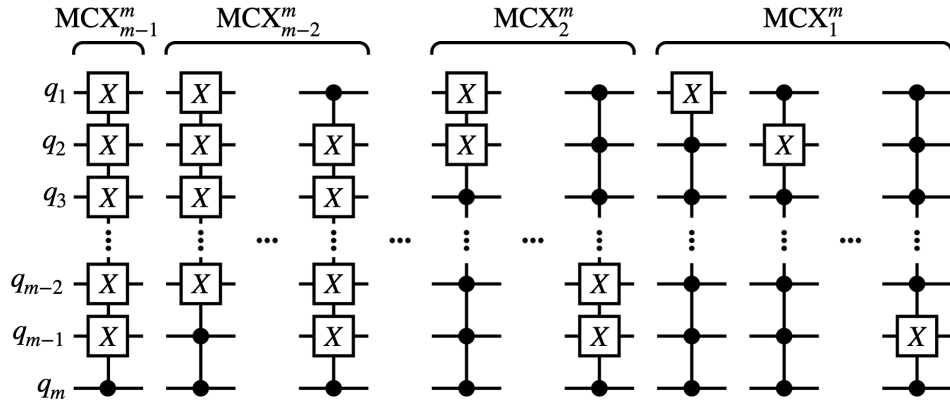


FIG. 14: The figure shows the types of $CX^{(x)}$ gates required for the Naimark measurement circuit acting on m qubits; in total, up to $2^{m-1} - 1$ such gates can act on m qubits. The m -bit string x are elements of the set $A(m)$. These $CX^{(x)}$ gates correspond to MCX gates, ranging from MCX_{m-1}^m to MCX_1^m . They are applied in increasing order of x , by selecting them sequentially from left to right in the figure. For $x = x_1 x_2 \cdots x_m$, $x_j = 0$ leads to an X gate on qubit q_j , whereas $x_j = 1$ leads to q_j serving as a control in the MCX gate. The two-outcome POVM circuit ($m = 1$) does not involve any $CX^{(x)}$ gates.

be decomposed into $48(m - 3)$ CNOTs. Therefore, the total number of CNOT gates is given by:

$$48k(\lfloor \log_2 i \rfloor - k - 2) \quad (\text{B1})$$

where $1 \leq k \leq \lfloor \log_2 i \rfloor$. This expression attain its maximum when $k = \frac{\lfloor \log_2 i \rfloor - 2}{2}$, yielding a maximum number of CNOT gates:

$$48 \left(\frac{\lfloor \log_2 i \rfloor - 2}{2} \right)^2. \quad (\text{B2})$$

By straightforward algebra, we obtain:

$$\mathcal{O}(48k(\lfloor \log_2 i \rfloor - k - 2)) = \mathcal{O}((\log_2 i)^2). \quad (\text{B3})$$

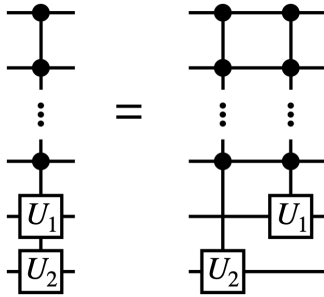


FIG. 15: Decomposition of multi-controlled U_1 and U_2 gates, where both unitaries are applied separately and controlled by the same set of qubits.

2. CNOT Count in the Uniformly Controlled Rotation Gate at the i -th B_{SA} Gate

The uniformly controlled rotation gate in the i -th B_{SA} gate has two types of controls: n system qubits that act as uniformly controlling qubits, and $\lfloor \log_2 i \rfloor$ ancillary qubits that act as standard control qubits.

As shown in Ref. [42], a uniformly controlled rotation gate with m uniformly controlling qubits is decomposed into 2^m single-qubit rotations and 2^m CNOT gates. Thus, using the decomposition scheme in Fig. 16, our gate is decomposed into 2^n multi-controlled rotation gates with $\lfloor \log_2 i \rfloor$ control qubits. Furthermore, the multi-controlled rotation gate with m control qubits can be decomposed into $2^m - 2$ CNOT gates and $2m$ single-qubit rotation gates [13]. Therefore, the total number of CNOT gates is given by

$$2^n(2^{\lfloor \log_2 i \rfloor} - 2). \quad (\text{B4})$$

3. CNOT Count in the V gate at the i -th B_{SA} Gate

A B_{SA} gate contains two V gates, each composed of n single-qubit rotation gates and $n - 1$ CNOT gates. Each V gate is controlled by $\lfloor \log_2 i \rfloor + 1$ qubits. We first consider the rotation gates, more precisely, multi-controlled rotation gates. Since a multi-controlled rotation gate with m control qubit is decomposed into $2^m - 2$ CNOT gates, the total number of CNOTs is given by

$$2n(2^{\lfloor \log_2 i \rfloor + 1} - 2) \quad (\text{B5})$$

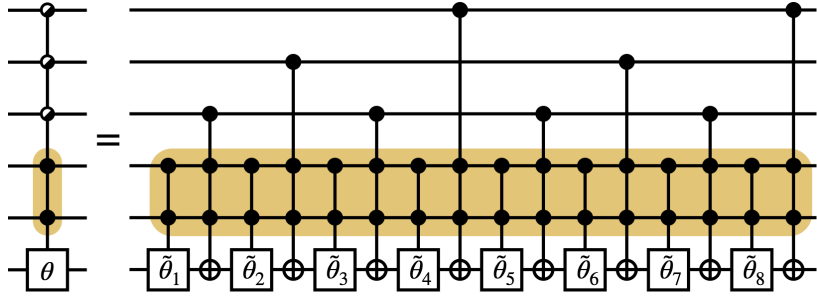


FIG. 16: Decomposition scheme of a uniformly controlled rotation gate with three uniformly controlling qubits and two additional control qubits. While the original decomposition of the uniformly controlled gate follows the method of [42], this figure illustrates how the gate structure extends when extra control qubits are included.

where the factor of 2 accounts for the two V gates in the B_{SA} gate.

We proceed to analyze the CNOT gates in the V gates, more precisely, $n - 1$ multi-controlled X gates with $\lceil \log_2 i \rceil + 2$ control qubits. From the previous discussion, there are a total of

$$96(n - 1)(\lceil \log_2 i \rceil - 1) \quad (\text{B6})$$

CNOTs, again including a factor of 2 for the two V gates in the B_{SA} gate.

Therefore, at the i -th B_{SA} gate and $CX^{(x)}$ gate, the uniformly controlled rotation gates dominate the CNOT count.

$$\mathcal{O}(2^n(2^{\lceil \log_2 i \rceil} - 2)) = \mathcal{O}(2^{n+1}i) \quad (\text{B7})$$

Summing over all B_{SA} gates yields

$$\sum_{i=1}^{l-1} \mathcal{O}(2^{n+1}i) = \mathcal{O}(2^{n+1}l^2) \quad (\text{B8})$$

Note that the single-qubit POVM requires $\mathcal{O}(l^2)$ CNOT gates [13], while the multi-qubit POVM involves

an additional multiplicative factor of 2^n due to the multi-qubit state on the system.

Appendix C: Total CNOT Count in the MCM Circuit

In this section, we analyze the CNOT count required to implement the circuit in Fig. 10 where the U_S is treated as a HEA. We consider two cases:

- *The case $l \leq 2^n$:* The circuit does not require any ancilla qubits.
- *The case $l > 2^n$:* The circuit requires $n_A = \lceil \log_2 l \rceil - n$ ancillary qubits, excluding Ancilla1 and Ancilla2 shown in Fig. 12.

After applying the BE gate on the system qubits, U_S acts on n qubits when $l \leq 2^n$, and $n + n_A$ qubits otherwise; hence, in general, U_S acts on $m = \max(n, \lceil \log_2 l \rceil)$ qubits. The O_K in the BE gate shown in Fig. 10 contains $4m^2$ CNOT gates by construction. In addition, each SWAP gate is decomposed into three CNOT gates, contributing $3m$ CNOTs. Furthermore, the HEA with L layers in U_S has $L(m - 1)$ CNOTs. Therefore, the CNOT count in the MCM circuit is $\mathcal{O}(m^2)$.